



LARGE SYNOPTIC SURVEY TELESCOPE

Large Synoptic Survey Telescope (LSST)

LSST Crowded Fields photometry

K. Suberlak, C. Slater, Ž. Ivezić

LSST-2017

Latest Revision: 2018-02-14

revision: TBD
status: draft

Abstract

A report on the performance of current LSST Stack pipelines in crowded stellar fields. Using the real data we explore the metrics that could be used to direct decision-making process for pipeline improvements. The quality metrics show also a way to validate the performance of LSST pipelines after major software upgrades.

Draft



Change Record

Version	Date	Description	Owner name
1	2017-07-16	First draft.	Krzysztof Suberlak
2	2017-10-19	Updated outline.	Krzysztof Suberlak
2	2018-01-25	Major revision.	Krzysztof Suberlak

Contents

1	Introduction	1
2	Identifying density regions	2
3	DECam Plane Survey	4
4	LSST Processing of DECAPS data	7
4.1	Cleaning DECAPS catalog, comparison to LSST pixel mask	7
4.2	Cleaning LSST catalog	8
5	Metrics	19
5.1	Completeness	19
5.2	Photometric accuracy	19
6	Future work	25
6.1	LSST Processing of StarFast Simulated Sky	25
6.2	Other LSST-DECAPS tests: w-color	28
6.3	Astrometry	28
A	Appendix A: TRILEGAL and DAOphot	32
A.1	DAOStarFinder source detection	32
A.2	TRILEGAL queries	32
A.3	Comparison of MAF, DAOStarFinder, and TRILEGAL counts	32

1 Introduction

We report on the performance of the Large Scale Synoptic Telescope (LSST) science pipelines¹, also known as 'the LSST stack', in stellar fields of varying levels of crowdedness.

The LSST will sample every night over 1,000 regions in the sky , delivering terabytes of raw data in need of processing: photometric and astrometric calibration, to deliver a calibrated exposure image, as well as a source catalog, among other image products² [7].

The survey sky is composed of regions very diverse in terms of stellar density, or crowdedness: from high density low-galactic latitude regions that have tens of millions of sources per square degree, to low-density regions towards the galactic poles with less than thousand sources per square degree.

Deblending and successful photometry is an inherent part of any astronomical data processing pipeline. There exists a body of research answering questions that are specific to crowded stellar fields, eg. how many beams do we need per source (see [2]), or how the crowded fields photometry can be approached in the era of large telescopes [8] Other studies involved eg. HyperSuprime CAM pipeline (developed in parallel with the LSST Stack), recognizing that the deeper the survey, the higher the stellar densities encountered, and the onset of blurring the boundaries between deblending, measurement, and detection [1].

In this report we compare the 'out-of-the-box' LSST Stack tools, in particular processCcd.py, to the DECAm [Galactic] Plane Survey (DECAPS) catalogs based on the NOAO state-of-the-art community pipeline ([9]). First we use the LSST Metrics Analysis Framework Galfast simulation of the night sky find regions representing various stellar densities - see Sec. 2. Then we query the DECAPS image database for images that were taken at exposures and filters that reach similar depth to the LSST single-visit depth (Sec. 3). We select few DECAPS exposures at each density level, and process with LSST Stack tools (Sec. 4). In Sec. 5 we compare the results of LSST processing and the DECAPS single-epoch catalogs, and develop the quality metrics. Finally in Sec. 6 we make recommendations for future work.

¹<https://pipelines.lsst.io>

²<http://ls.st/LSE-163>

2 Identifying density regions

To identify regions representing different stellar densities we use the LSST Metrics Analysis Framework³ simulated stellar density map prepared by P. Yoachim and L. Jones⁴

The resulting dataset starDensity_r_nside_64.npz contains 64 magnitude bins, with the entire sky divided into 49152 healpixels⁵. Each healpixel contains information about the number of stars per square degree in a given magnitude bin in the simulated sky - see Fig. 1.

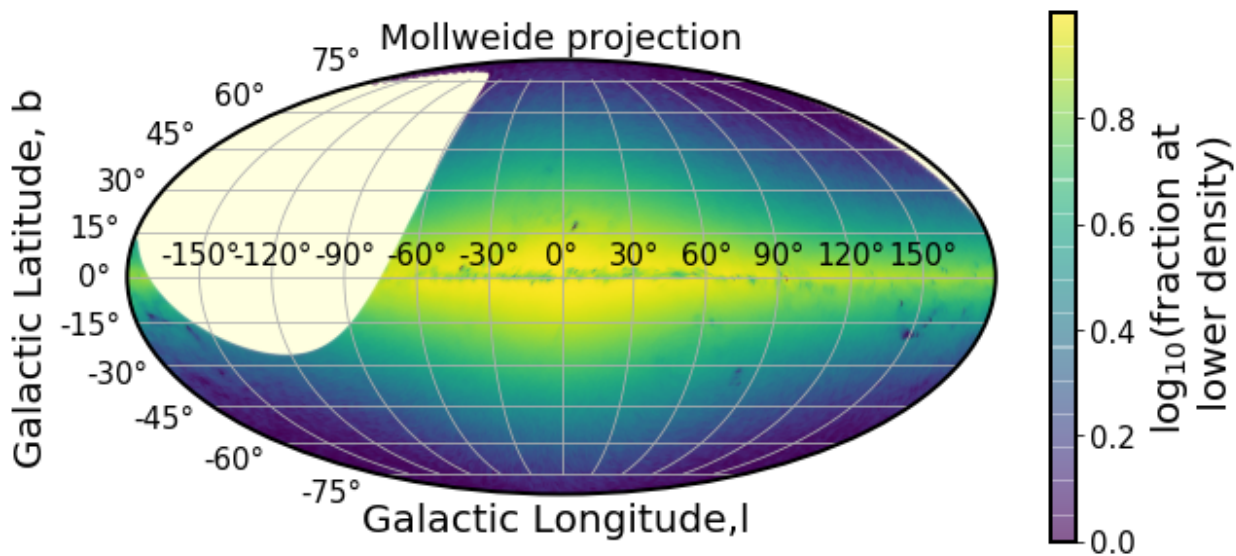


FIGURE 1: MAF healpixels plotted in galactic coordinates in Mollweide projection. The brightest regions correspond to highest stellar densities. The missing part in the higher declination is the part of the sky above $\delta > 40^\circ$, which is not observable from the southern location of Cerro Pachón.

To match the LSST single-visit depth, we select magnitude bins smaller than $r=24.5$. For each healpixel we calculate the number of pixels that have a higher stellar count. Since each healpixel has an equal area, the fraction of pixel number above a certain threshold corresponds to the fraction of sky area above given density limit. Fig. 2 illustrates how we define percentiles of stellar densities, so that eg. 'top 1%' density means that only 1 in 100 pixels has a higher density than a given pixel, and 'top 10%' means that '10 %' of pixels in the considered simulation of the sky.

³<https://www.lsst.org/scientists/simulations/maf>, and https://github.com/lsst/sims_maf

⁴[sims_maf/python/lsst/sims/maf/maps/createStarDensitymap.py](https://github.com/lsst/sims_maf/blob/python/lsst/sims/maf/maps/createStarDensitymap.py)

⁵<http://healpix.sourceforge.net>

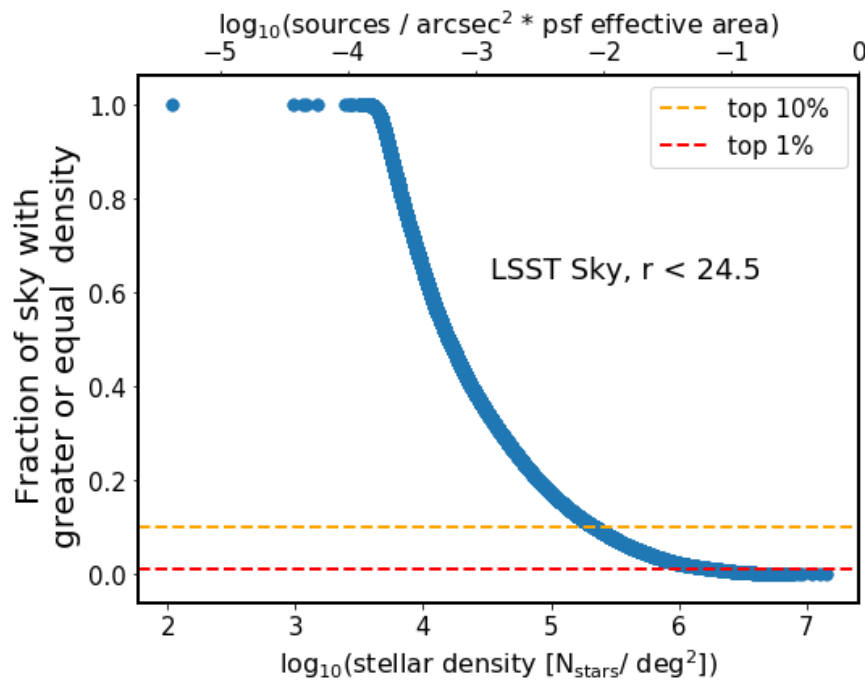


FIGURE 2: Stellar density as a function of the fraction of the LSST simulated sky at greater or equal density. For each healpixel in the Galfast simulation we find the number of pixels at greater or equal stellar count, which corresponds to the area of the sky at greater density. Normalizing that by the total number of pixels we obtain a fraction of the sky at greater or equal density, similar to the cumulative distribution. Horizontal dashed lines illustrate selecting pixels at 1% or 10% density. From this plot we read that about 1% of the sky has more than 10^6 stars per sq.deg. . The 5% level corresponds to about 200000 stars per sq.deg. The second x-axis displays the density expressed as in terms of dimensionless quantity $N_{\text{beam}} = N_{\text{stars}}/\text{arcsec}^2 * A_{\text{PSF}}$, with the PSF effective area $A_{\text{PSF}} = \pi r^2$, assuming that diameter of the psf effective area is ≈ 0.8 FWHM, and the radius is 0.4 arcseconds.

Since this definition of density includes all pixels that are within 'top 20%', we take selection around the percentiles so that :

- top 1 % means fraction of sky with greater density is 0.01
- 5 % region means such that between 4% and 6%
- 20 % region includes 19% - 21%
- 50 % region includes 49% - 51%

We illustrate the location of pixels representative of these density brackets on the sky in Fig. 3.

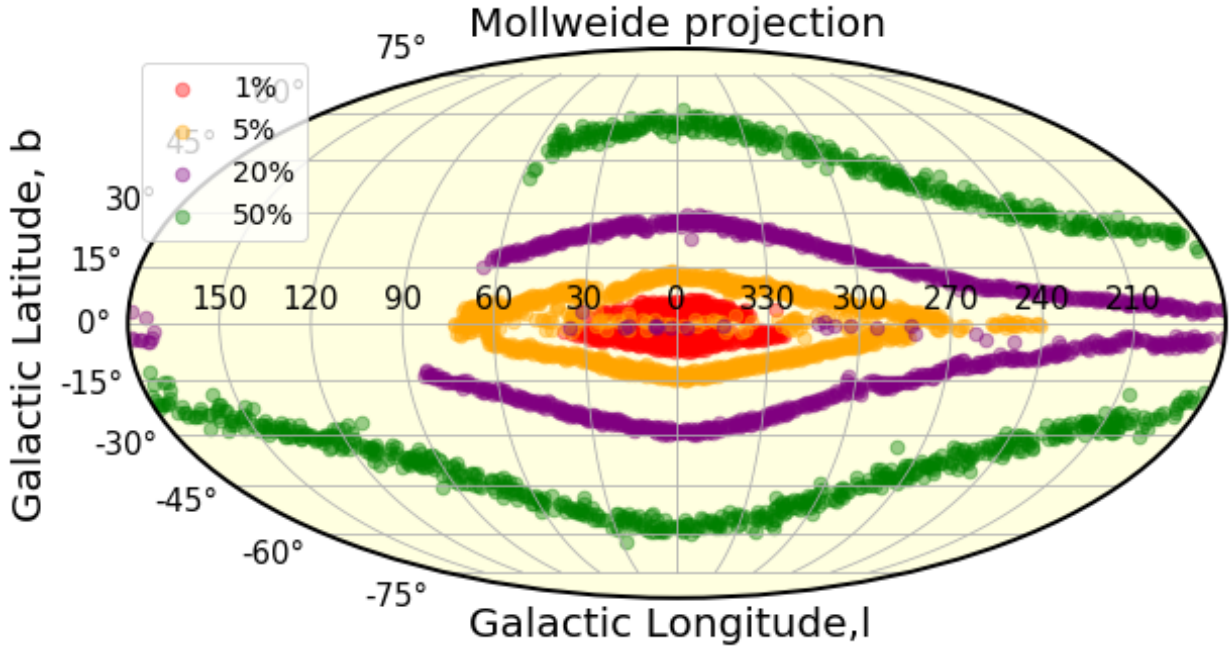


FIGURE 3: Illustration of location of regions representative of different relative density in cylindrical projection, galactic coordinates. The highest density regions are located close to the galactic bulge, and the decreasing density regions approximately trace isophotes of the Milky Way. The 20% regions close to the galactic equator correspond to high extinction regions that appear to have less counts due to interstellar dust.

3 DECam Plane Survey

To analyze the performance of the LSST Stack with real data, we used the Dark Energy Camera (DECam) imaging, taken as part of the DECam Plane Survey (DECAPS) [9], at the 4-m Cerro

Tololo Inter-American Observatory telescope (CTIO)⁶. On Fig. 4 we overlay the locations of all DECAPS fields on top the MAF map of the LSST sky. All DECAPS single-epoch images were processed with the DECAPS pipeline, resulting in single-epoch catalogs. The headers of all catalogs were assembled into the image database that contains information about single-visit exposure time, filter, time of observation, position, etc. It was used to select DECAPS fields with single-epoch depth similar to that of the single-visit depth of 30 sec LSST exposure. Thus we selected DECAPS fields with exposure between 90 and 125 sec, taken in u, g, r, or VR filter.

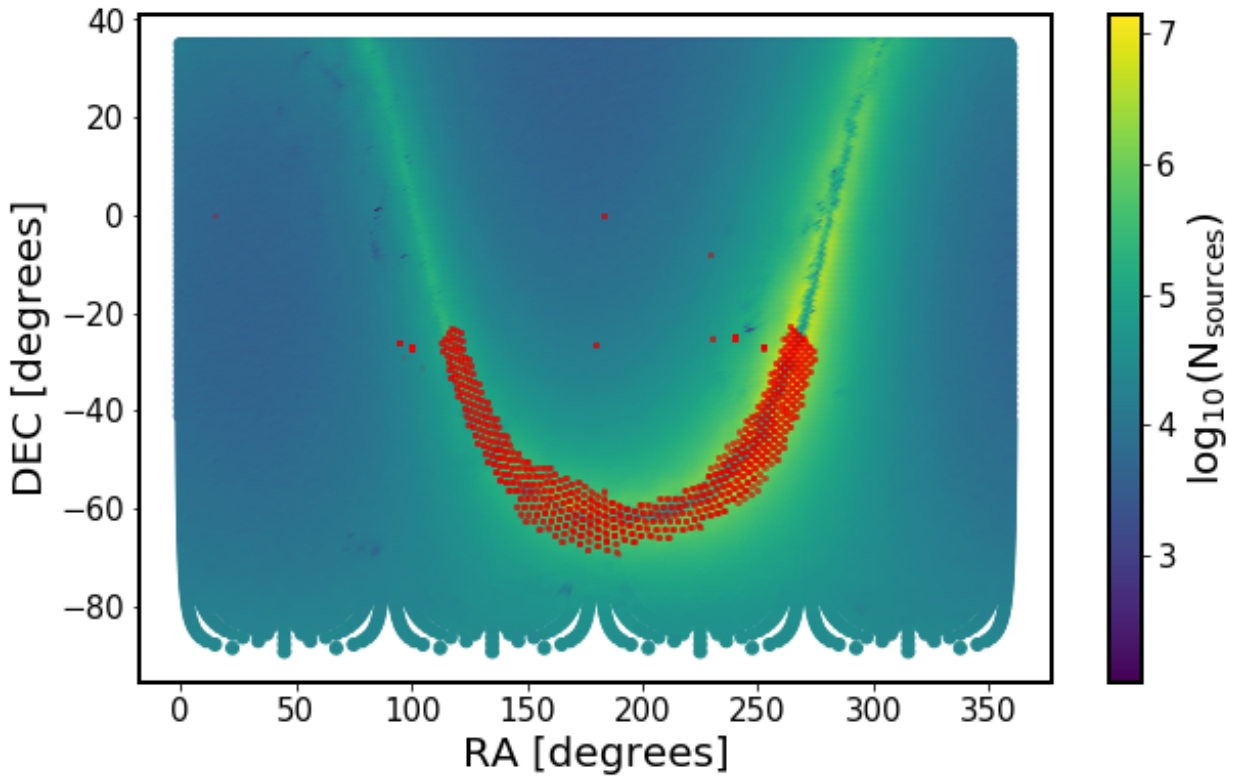


FIGURE 4: All DECAPS fields, overlaid on the map of healpixel stellar densities from MAF simulated sky. We matched the position of the center of each DECAPS field to the nearest healpixel to obtain an estimate of stellar density at each DECAPS field. In this way we selected DECAPS fields representative of various stellar densities (eg. 5%, 10%, 15%, as explained in Sec. 2).

We cross-matched the DECAPS image database with the stellar density information contained in MAF healpixels. Each DECAPS image plane is tiled by a mosaic of 62 CCDs (see Fig. 5). The size of each CCD element of the DECam image plane mosaic is 2046x4094 pixels, with pixel scale of 0.27 arcsec / px, so that a single mosaic element covers an area of 0.047117 square °. A single DECam exposure is also called a visit, and with 62 mosaic elements the full field of

⁶see <http://www.ctio.noao.edu/noao/node/1033>

view 2.2° wide is several times bigger than the full moon. This makes it comparable to the LSST 3.5° wide field of view. Using the coordinates of the center of each DECAPS field we found the nearest healpixel within 0.5° .

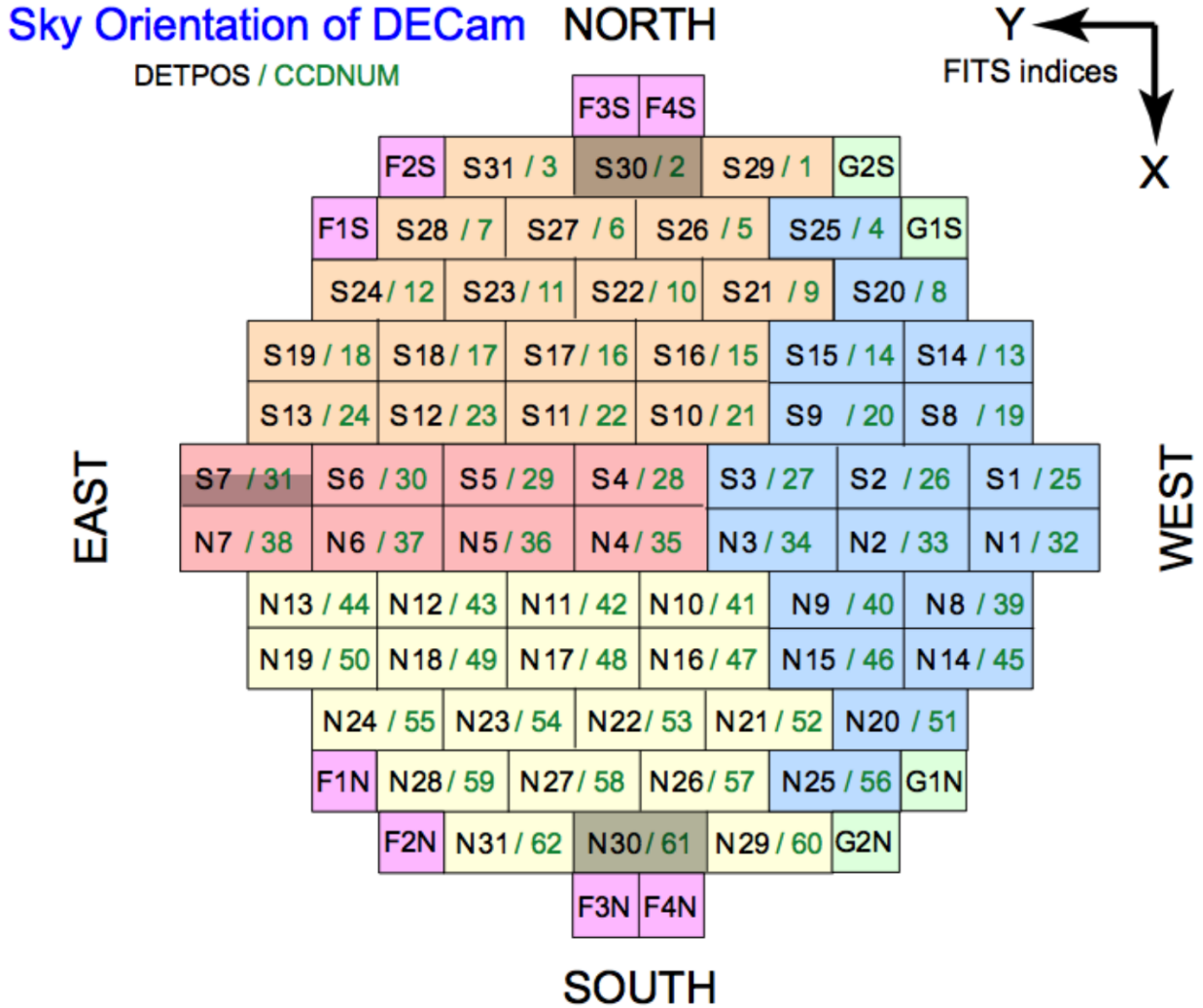


FIGURE 5: An illustration of the DECam CCD mosaic image plane, adapted from Fig.4-3 in NOAO Data Handbook [10]. The color corresponds to the one of the four sets of read-out electronics (orange,pink,blue,yellow), or the guiding (green) and focus (magenta) CCDS. The grey CCDs do not function properly. For this reason S30, S7, and N30 were excluded from the analysis.

TABLE 2: LSST pixel mask bit values.

Bit position	Description	Mask decimal value
0	bad	1
1	saturated	2
2	interpolated	4
3	cosmic ray	8
4	edge	16
5	detected	32
6	detected negative	64
7	suspect	128
8	no data	256

4 LSST Processing of DECAPS data

The DECAPS calibrated imaging was processed with the LSST Science Pipelines installed on the LSST-dev machine installed at the NCSA. We specifically employed processCcd.py and the standard Stack configuration. Transferring the resulting source catalogs and calexp files over scp we analyzed the output on a laptop with jupyter notebooks.

To obtain independent order of magnitude comparison to MAF simulation, and LSST/DECAPS processing of DECam data, we also queried TRILEGAL simulation data, and processed the DECam images with DAOPhot - see Appendix A.

The big picture is to find how metrics that we develop behave as a function of source crowdedness. We consider completeness, and photometric accuracy.

4.1 Cleaning DECAPS catalog, comparison to LSST pixel mask

To compare LSST and DECAPS catalogs, we cleaned both catalogs with the flags assigned to each source by the respective image processing pipeline. To verify the validity of DECAPS source flags, we compared them with the LSST pixel-level mask information stored in the FITS Header Data Unit. Pixel-level masks are encoded in 8 bits, each of which can be 'on' or 'off', signifying that a given flag was 'on' or 'off' for a given pixel. The total value of the mask at each pixel is a decimal representation of such eight bits binary number, eg. $(00100001)_2 = 2^0 + 2^5 = 1 + 32 = (33)_{10}$ means that bit '0' and '5' are 'on' (counting from the right). See Table 2 for details.

TABLE 3: DECAPS flags. We excluded sources with flag bits 1,3,4,5,6,8,20,22.

Bit position	Description
1	Bad pixel
3	Saturated
4	Bleed trail
5	Cosmic ray
6	Low weight
8	Long streak
20	Additional bad pixel
21	Nebulosity
22	S7 amplifier B

For each visit we considered DECAPS single-epoch source catalog, and the LSST calexp image. For each DECAPS source, given the pixel coordinates, we retrieved the value of the LSST mask at that pixel. Given the understanding of the LSST flag bits (Table 2) we performed a bitwise and with a mask filter $(1101111)_2 = (2^1 + 2^2 + 2^3 + 2^4 + 2^6 + 2^7)_{10}$, flagging a source as 'lsst bad' if either of the flag bits apart from '5' (detected) was 'on'.

Each DECAPS source also has a flag where the value is composed of bits inherited from the NOAO Community Pipeline and new flags(see Table 3). We performed a bitwise and with the mask filter $(2^1 + 2^3 + 2^4 + 2^5 + 2^6 + 2^8 + 2^{20} + 2^{22})_{10}$, flagging the source as 'decaps bad' if either of this bits were 'on'. We compared which sources would be excluded based on the DECAPS source-level flags vs LSST pixel-level masks, and we found that for a particular visit 611980 the overlap between sources excluded based on LSST pixel mask vs DECAPS source flags is 99%. This means that DECAPS flagging is consistent with the LSST mask information, and the same sources would be 'excluded' based on either DECAPS flags or LSST mask information. For this reason we cleaned the DECAPS catalog with source level flags.

4.2 Cleaning LSST catalog

The LSST source catalog contains per source a list of 83 flags that could be set 'on' or 'off'. Of these, flags number 60:72 are base_PixelFlags_flag, meaning they contain information relevant to the level of source detection, rather than processing. See Table 4 for detailed description.

We clean the LSST source catalog from sources that have flags number 62 (edge) or 67 (inter-

TABLE 4: LSST source flags explanation. All flags names start with 'base_PixelFlags_flag' which was omitted in the flag_name column below.

number	name	explanation
60	flag	general failure flag, set if anything went wrong
61	offimage	Source center is off image
62	edge	Source is outside usable exposure region (masked EDGE or NO_DATA)
63	interpolated	Interpolated pixel in the Source footprint
64	saturated	Saturated pixel in the Source footprint
65	cr	Cosmic ray in the Source footprint
66	bad	Bad pixel in the Source footprint
67	suspect	Source's footprint includes suspect pixels
68	interpolatedCenter	Interpolated pixel in the Source center
69	saturatedCenter	Saturated pixel in the Source center
70	crCenter	Cosmic ray in the Source center
71	suspectCenter	Source's center is close to suspect pixels
72	flag	General Failure Flag

polatedCenter)⁷. Other flags would remove too many sources that have only small 'defects', eg. 64 (interpolated) is on for a bright source on the footprint of which there is a cosmic ray, and 65 (bad) is on for any source which has even one bad pixel in the footprint -see Fig. 6. A comparison of the starting source count and final source count (after cleaning) is shown on Fig. 7, and Table 5

Given the single-epoch DECAPS source catalogs, and the LSST source catalogs, we followed a uniform set of procedures to clean both datasets, and in turn cross-match positionally. First we made a quality cut removing all sources with signal-to-noise ratio smaller than five: $S/N < 5$. The number of sources thus removed depends on a visit number, but does not exceed few % of the catalog. Following that we also removed sources with flags that correspond to bad, edge detections, cosmic rays, or saturation spikes (as outlined in Sec. 4.1 and 4.2). The LSST Processing Pipeline deblends sources in a similar fashion to the SDSS Imaging Pipeline⁸. For the LSST source catalog, we chose to keep only those sources that were either isolated parents (parentId=0, nchild=0), or deblended children (parentId != 0 , nchild=0) (see Table 7 for details.)

We illustrate the DECAPS-LSST 'matches' and 'mismatches' for visit 611980 CCD01 on Figs. 8, 9, and CCD10 on Figs. 10, 11 and 12

⁷This is similar to the example in Sec.4 of SDSS Image Processing I: The Deblender [3]

⁸SDSS Image Processing I: The Deblender [3], SDSS Image Processing II: The Photo Pipelines [4], [6], and [5]

TABLE 5: A summary of all LSST-processed DECAPS visits. The column ‘visit’ corresponds to the DECAPS visit number. The following four columns (‘N raw’, ‘N f’, ‘-N r’, ‘=N c’) contain the source counts per visit area ($\approx 2.74 \text{ deg}^2$). ‘N raw’ is the input number of sources per visit , summing over all CCD source catalogs. ‘(N f)’ is the number of sources removed due to bad flags. ‘-N r’ is the total number of removed sources (due to flags, low S/N, or sources that in the LSST deblending process are neither isolated parents, nor deblended children). ‘=N c’ is the final number of clean sources per visit (‘N raw’ - ‘N r’= ‘N c’). ‘N c/deg²’ is ‘=N c’ converted to count per deg². N MAF/deg² is the predicted number of sources per deg² at that location based on Galfast simulation. ρ_{MAF} is the MAF density; eg. 21.3 is the top 21.3% stellar density of the simulated sky.

Visit	N raw	(N f)	-N r	=N c	N c/deg ²	N MAF/deg ²	ρ_{MAF}
568172	29809	9148	12434	17375	21.3	72072	6241
527319	120862	13744	39638	81224	19.9	79632	29175
530012	160406	15210	61337	99069	10.6	203040	35585
525846	167582	15247	63295	104287	10.6	203040	37459
525900	171337	15037	58219	113118	19.9	79632	40631
529989	182933	15910	61808	121125	19.9	79632	43508
529974	228849	16842	67339	161510	20.5	76572	58014
525814	235307	16811	72214	163093	20.5	76572	58582
527096	227256	16100	59686	167570	25.0	55908	60191
644125	242521	16387	72363	170158	21.3	72072	60101
611980	273032	18816	76043	196989	15.6	116856	70758
527247	264383	15283	66539	197844	15.6	116676	71065
567283	280305	16981	68379	211926	4.0	612648	76123
527246	319929	18136	86268	233661	15.7	114588	83930
640891	355861	24520	107462	248399	15.1	121536	87737
611970	377917	26716	120640	257277	11.5	178992	92413
645251	348033	18786	89669	258364	14.7	128016	91257
527296	361951	21167	101452	260499	4.2	588096	93571
611969	387056	25752	118639	268417	7.9	292788	96415
526413	368017	22267	98745	269272	20.1	78480	96722
525838	371329	19984	100644	270685	15.6	116676	97229
525837	393879	22350	107414	286465	15.7	114588	102898
611529	398924	22625	105677	293247	15.6	116856	105334
525920	415231	22439	111423	303808	4.2	588096	109127
527300	436689	24839	120330	316359	4.2	594324	113635
525904	479294	26679	135534	343760	4.2	594324	123478
527453	495629	28732	139172	356457	9.3	242316	128039
609754	490143	26233	121738	368405	15.6	116856	132330
530032	486203	23112	115217	370986	10.7	198432	133257
526152	520842	28739	143336	377506	25.1	55404	135599
567795	508405	26663	129592	378813	3.4	721728	136069
641497	529827	28546	137626	392201	10.5	205308	138530
527064	558264	26197	132299	425965	4.2	591336	153006
525879	575982	28502	139102	436880	10.7	198432	156927
644144	597726	30439	152632	445094	1.7	1292976	168442
644082	614401	29828	152226	462175	3.0	783324	163246
526028	911721	38810	234490	677231	7.7	305280	243260
644074	916795	41973	219530	697265	5.1	481788	246282
641548	1005146	44347	238787	766359	6.7	355896	270687

TABLE 6: A summary of all single-epoch DECAPS source catalogs, with columns as in Table 5. See Fig. 7 comparing the 'N raw' converted to number of sources per square degree, and 'N clean per sq.deg.'

Visit	N raw	(N f)	-N r	=N c	N c/deg ²	N MAF/deg ²	ρ_{MAF}
568172	16824	138	150	16674	21.3	72072	5989
527319	92326	2819	3039	89287	19.9	79632	32071
530012	121313	3293	3982	117331	10.6	203040	42145
525846	125245	3135	3457	121788	10.6	203040	43746
525900	127722	2557	2786	124936	19.9	79632	44876
529989	140043	2527	2803	137240	19.9	79632	49296
527096	194837	2126	2290	192547	25.0	55908	69162
525814	200562	4481	4938	195624	20.5	76572	70268
529974	224231	3992	4413	219818	20.5	76572	78958
644125	228088	5570	6182	221906	21.3	72072	78380
527247	237656	4858	5144	232512	15.6	116676	83518
527246	301083	5469	5907	295176	15.7	114588	106027
611980	315722	6779	7397	308325	15.6	116856	110750
527296	330295	7176	7726	322569	4.2	588096	115866
611970	340528	9668	10513	330015	11.5	178992	118541
645251	343358	5546	6253	337105	14.7	128016	119069
640891	361837	9423	10389	351448	15.1	121536	124135
525838	360793	6057	6515	354278	15.6	116676	127256
611969	376588	10280	11243	365345	7.9	292788	131231
527300	409385	8974	9654	399731	4.2	594324	143583
611529	428299	9981	11167	417132	15.6	116856	149833
525837	425261	6791	7437	417824	15.7	114588	150082
526413	428035	8417	9137	418898	20.1	78480	150467
525920	449868	6675	7430	442438	4.2	588096	158923
609754	474355	10034	11677	462678	15.6	116856	166193
525904	490306	8413	9118	481188	4.2	594324	172842
567283	575760	5549	6426	569334	4.0	612648	204504
526152	599164	12579	14023	585141	25.1	55404	210182
641497	611424	10156	11324	600100	10.5	205308	211962
530032	638179	9776	10964	627215	10.7	198432	225295
527453	682113	14654	16569	665544	9.3	242316	239062
525879	772457	11625	13117	759340	10.7	198432	272754
567795	791019	9439	11056	779963	3.4	721728	280162
644082	1007998	12826	15633	992365	3.0	783324	350515
526028	1035808	17929	20772	1015036	7.7	305280	364600
527064	1085375	10200	12399	1072976	4.2	591336	385412
641548	1404895	14336	17562	1387333	6.7	355896	490023
644144	1444897	16255	28641	1416256	1.7	1292976	535971
644074	1692430	16941	23670	1668760	5.1	481788	589427

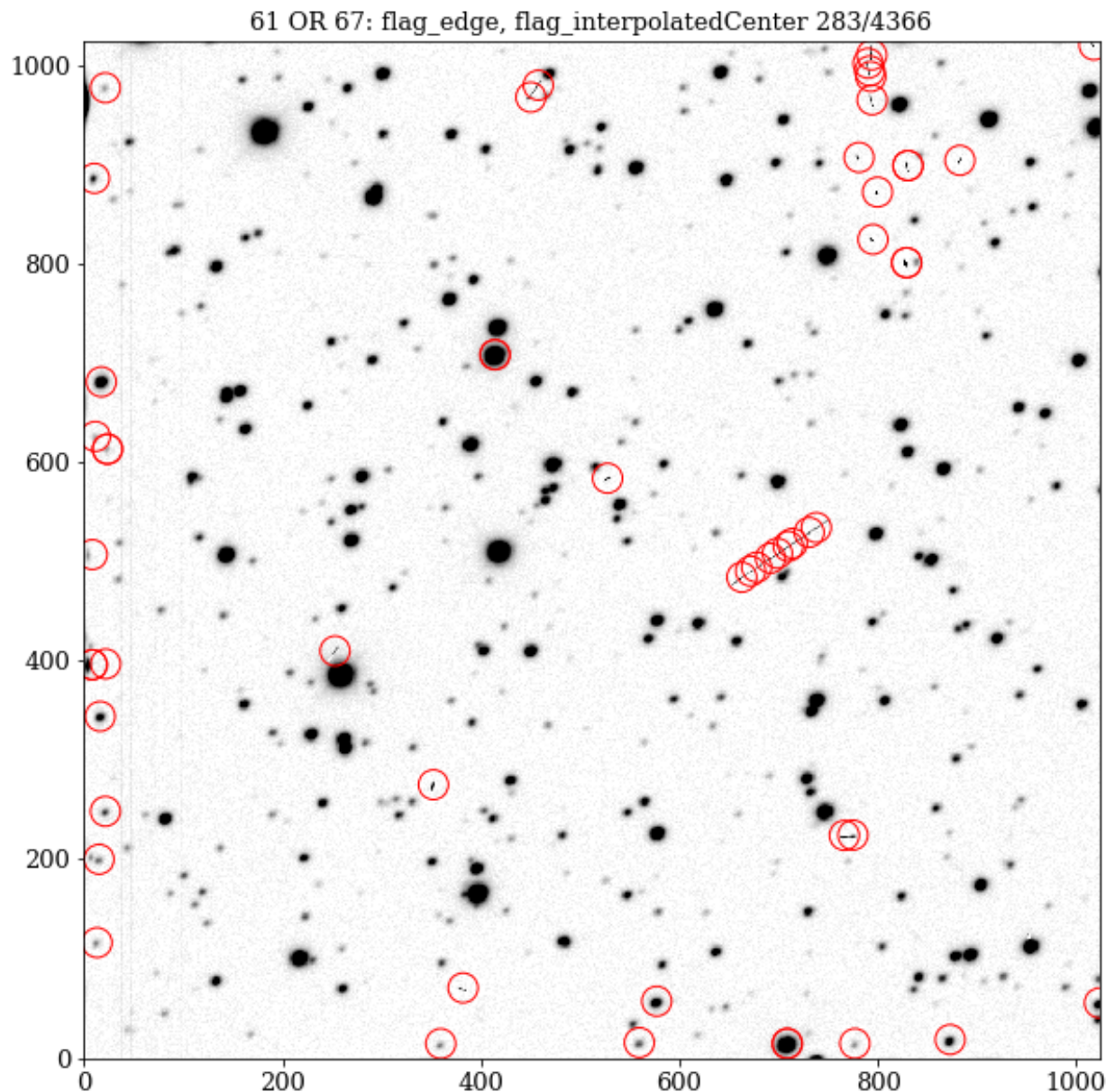


FIGURE 6: Sources from LSST source catalog for CCD 01 , visit 611980, for which flags 61 or 67 were 'on'. This cleans sources that were either on the CCD edge, or have been interpolated at the center. This properly removes the cosmic rays and edges, while preserving other sources that may have eg. a single bad pixel , or cosmic ray going across the footprint.

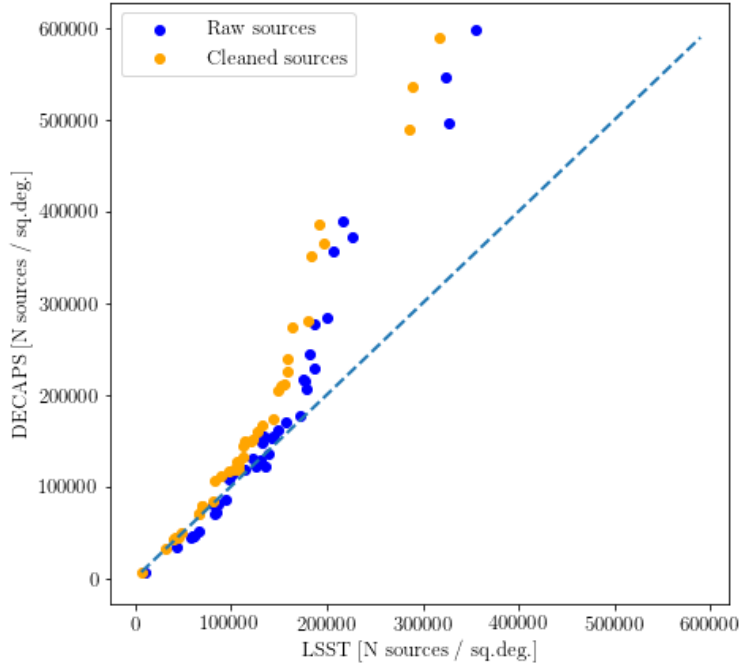


FIGURE 7: A plot of source count comparing LSST to DECAPS source catalogs of the same fields (visits). Blue dots mark raw source count, i.e. count of the input LSST source catalog or DECAPS single-epoch catalog. The source catalog count was converted to number of sources per square degree, due to the fact that in some cases not all CCDs were processed (e.g. visit 611144 in the top 1% region, where with CCDs 54,55,59,61 the LSST Pipeline suffered from the memory overflow). Orange dots mark the count of clean sources, after removing the low S/N sources, and those with ‘bad’ flags (see Fig. 6). As we would expect, between raw and clean catalogs the points on the diagram move vertically from top to bottom, and horizontally from right to left. For exact counts in each stellar field, see LSST counts Table 5 and DECAPS counts Table 6

TABLE 7: Summary of possible parentId and nchild combinations for blended sources in the LSST Science Pipeline. An example count in the final column is provided for visit 525814, a top 20% density region, which has the raw source count 235307. For that visit 16811 sources had bad flags, 49901 had $S/N < 5$, and in total 163093 were kept in the clean catalog.

parentId	nchild	type	decision	count
0	0	parent: isolated source	keep	104406
0	>0	blended source	remove	26981
!=0	0	deblended child	keep	103920
!=0	>0	failure case	remove	0

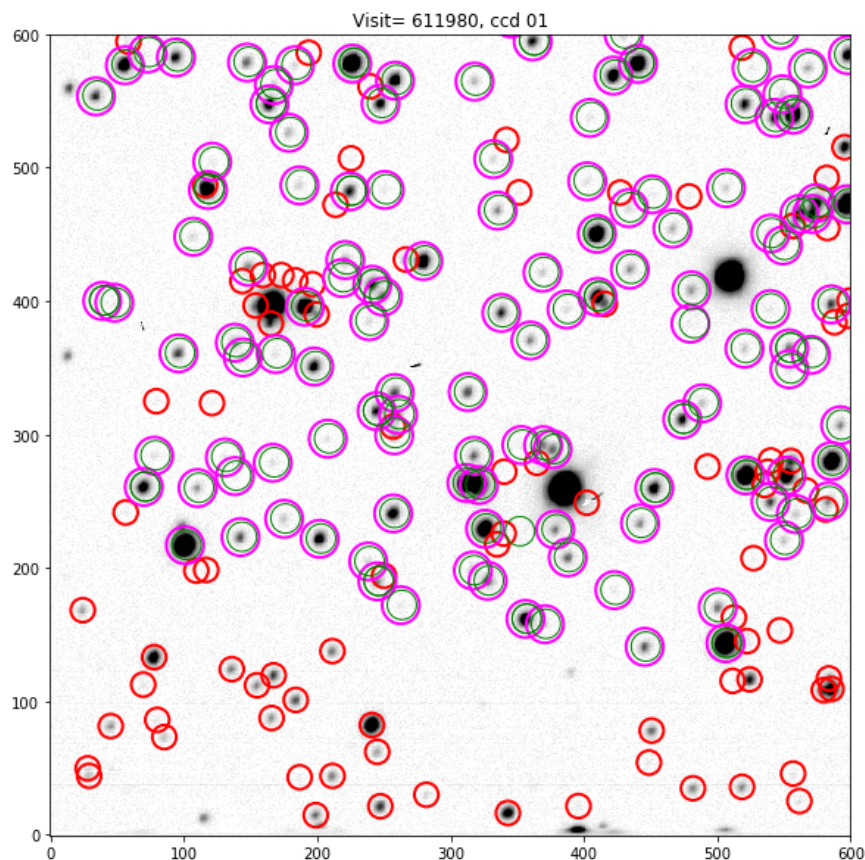


FIGURE 8: We consider cleaned DECAPS and LSST catalogs. All LSST sources are marked in green, and all DECAPS sources with an LSST counterpart are marked in magenta. The DECAPS sources missing LSST counterpart within 0.5 " are shown in red.

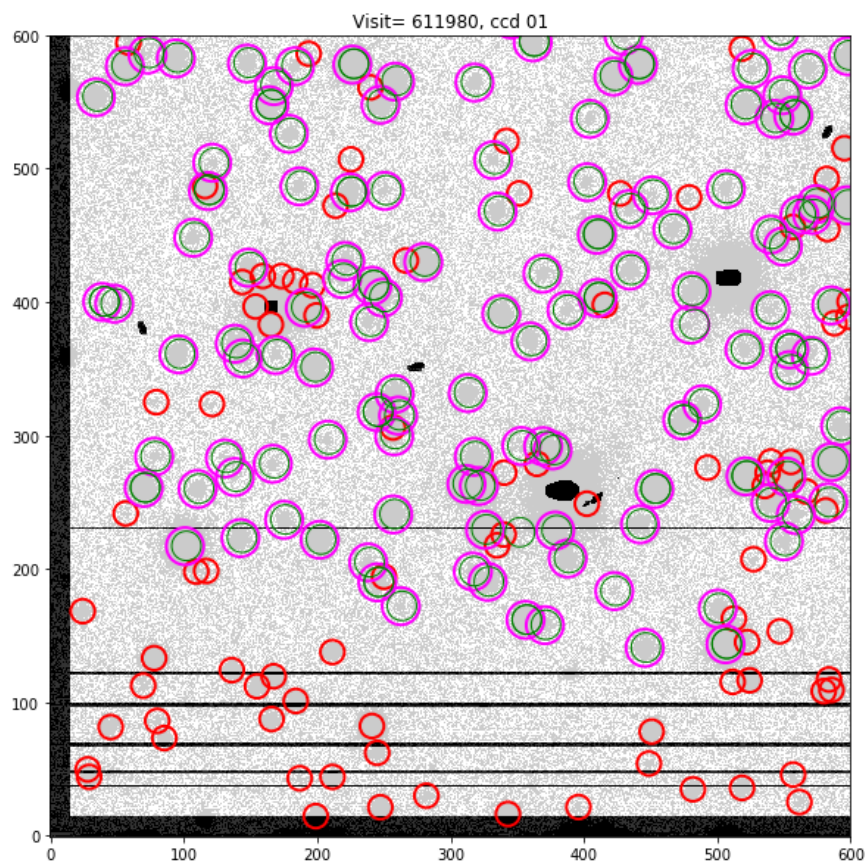


FIGURE 9: The same as Fig. 8, but showing the LSST pixels that have bits 0,1,2,3,4,6,7,8 'on' in dark shading (see Tab. 2). In particular, the horizontal stripes on the bottom correspond to bit 0 ('bad').

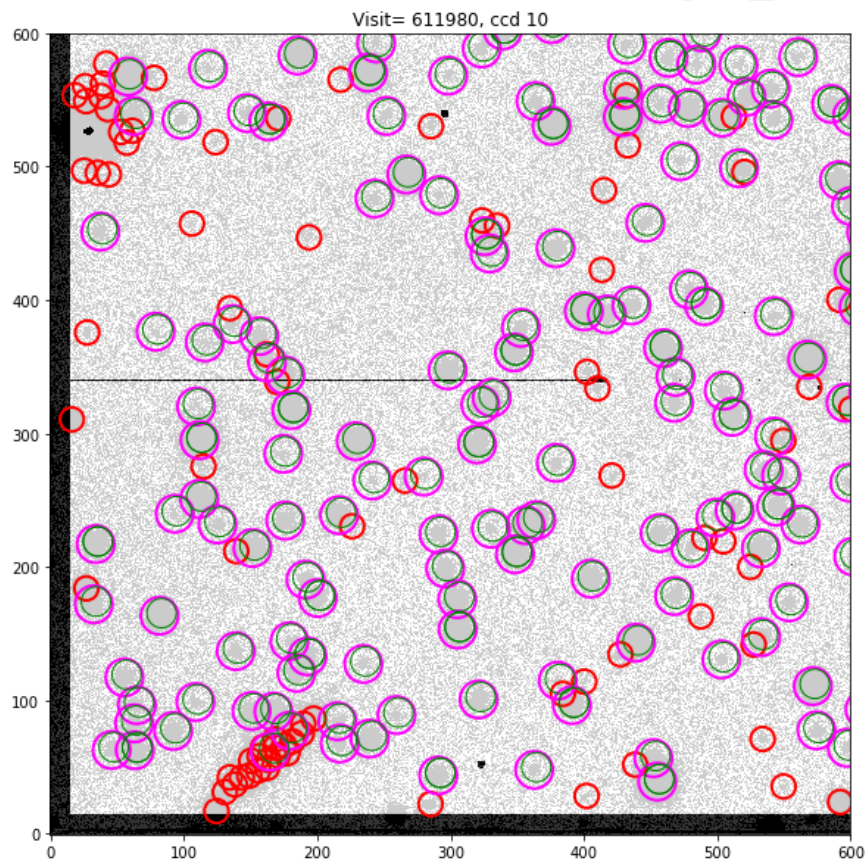


FIGURE 10: Like on Fig. 9 we overlay the LSST pixel mask data on top DECAPS sources that do (magenta) and do not (red) have an LSST counterpart within 0.5 ‐.

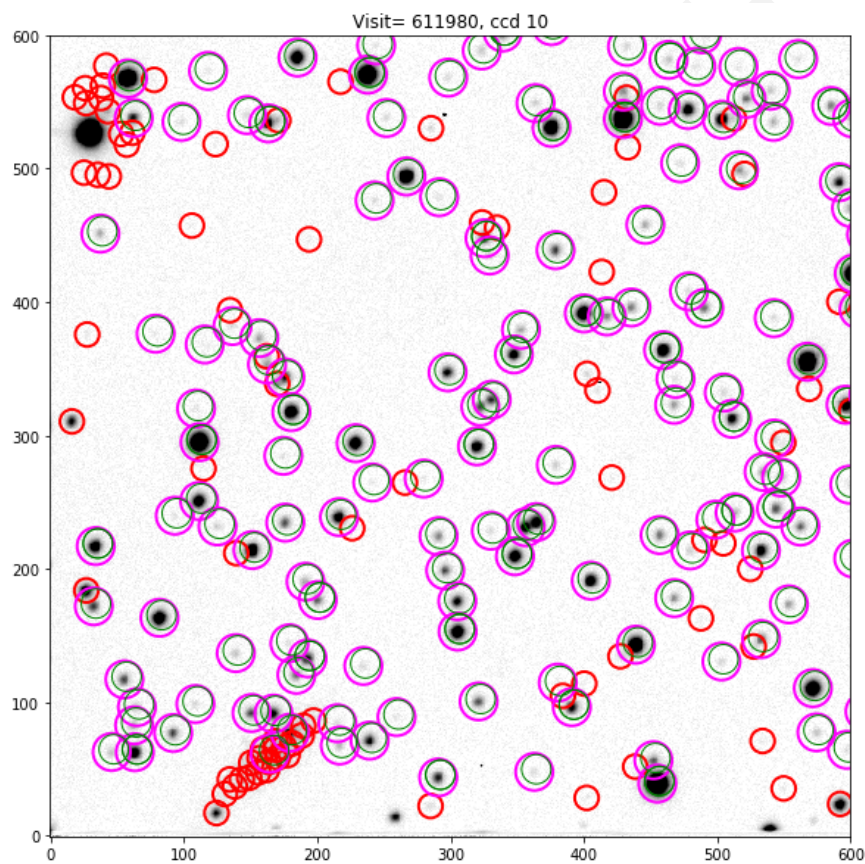


FIGURE 11: The same region of visit 611980, CCD10, as Fig. 10, showing all LSST sources, as well as DECAPS sources that do (magenta), and do not (red) have an LSST match.

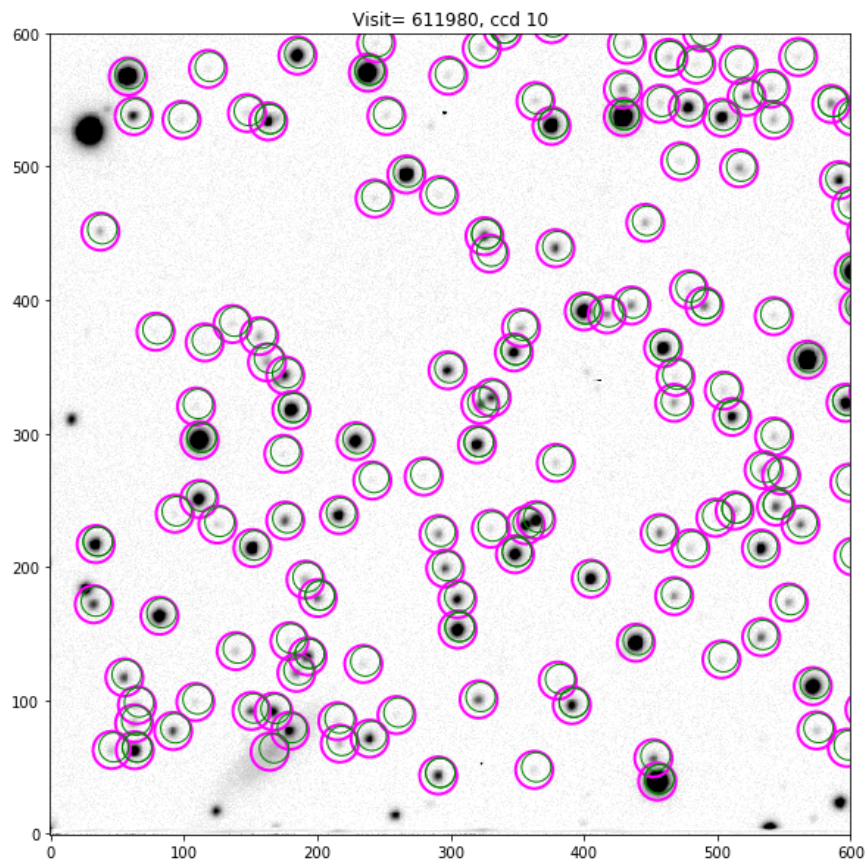


FIGURE 12: Compare to Fig. 11 - here we marked only the DECAPS sources that have an LSST match within $0.5''$, and all LSST sources, removing the red DECAPS sources that did not have an LSST match. This allows to notice the galaxy in the lower left corner that was shredded by DECAPS pipeline to point sources.

5 Metrics

Starting with cleaned LSST and DECAPS source catalogs, we consider a set of metrics to compare the quality of LSST science pipelines to the state-of-the-art DECAPS pipeline.

5.1 Completeness

For each visit that corresponds to a given level of crowdedness, consider the detection completeness of the LSST to the DECAPS sources. Assuming that DECAPS is the ‘true’ catalog of sources, the completeness is defined by the percentage of DECAPS sources (binned along DECAPS magnitude), that have an LSST match.

Given two catalogs, each with a set of source coordinates and photometry, one catalog is positionally cross-matched to another. This means that for each source of the first catalog is paired to the nearest source in the other catalog. The spatial separation and magnitude difference are two quantities that we choose as the basis of comparison. First, we require that to be called a ‘match’ the sources in two catalogs must have coordinates that differ by not more than $0.5''$. This is a very liberal cut given that the peak of the separation histogram occurs at distance smaller than $0.3''$ for $>98\%$ of sources in all visits (see Fig. 13). Second, we require that the sources differ by not more than 0.5 magnitudes. As illustrated on Fig. 15, this only removes the outliers. In fact, given that the majority of the sources ($>98\%$) that are matched within $0.5''$, and do not differ by more than 0.5 magnitude, this constraint does not change the completeness by more than few %. Fig. 14) shows how completeness , and catalog counts, depend on source density (from LSST catalog).

5.2 Photometric accuracy

We also considered the photometric accuracy. Since both DECAPS and LSST processing pipelines start from the same instcal calibrated DECam images, they ought arrive at similar measurement of flux, and in turn, magnitudes. The fact that there exists an offset and a spread in magnitude difference corresponds to slight differences in the details of each processing pipeline. We compare both the photometric difference between same fields processed by two different pipelines: DECAPS to LSST. Assuming that the majority of objects are non-variable in nature, we consider consecutive observations of the same stellar field at different epochs, to find the statistical variance epoch-to-epoch, thus resulting in DECAPS-DECAPS and LSST-LSST compar-

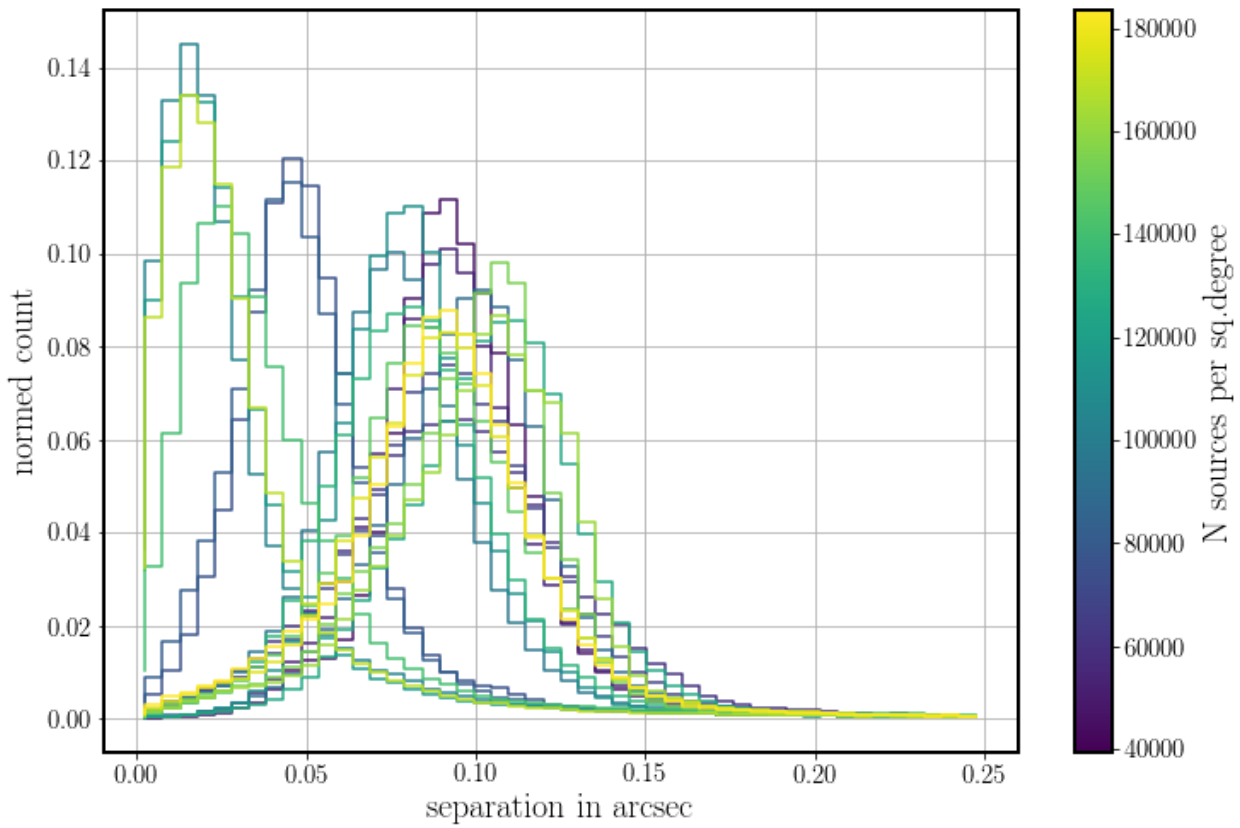


FIGURE 13: The histogram of separation of cross-matched sources between LSST and DE-CAPS catalogs for visits at various source densities. For all visits the peak of source separation is well within 0.5 "limit.

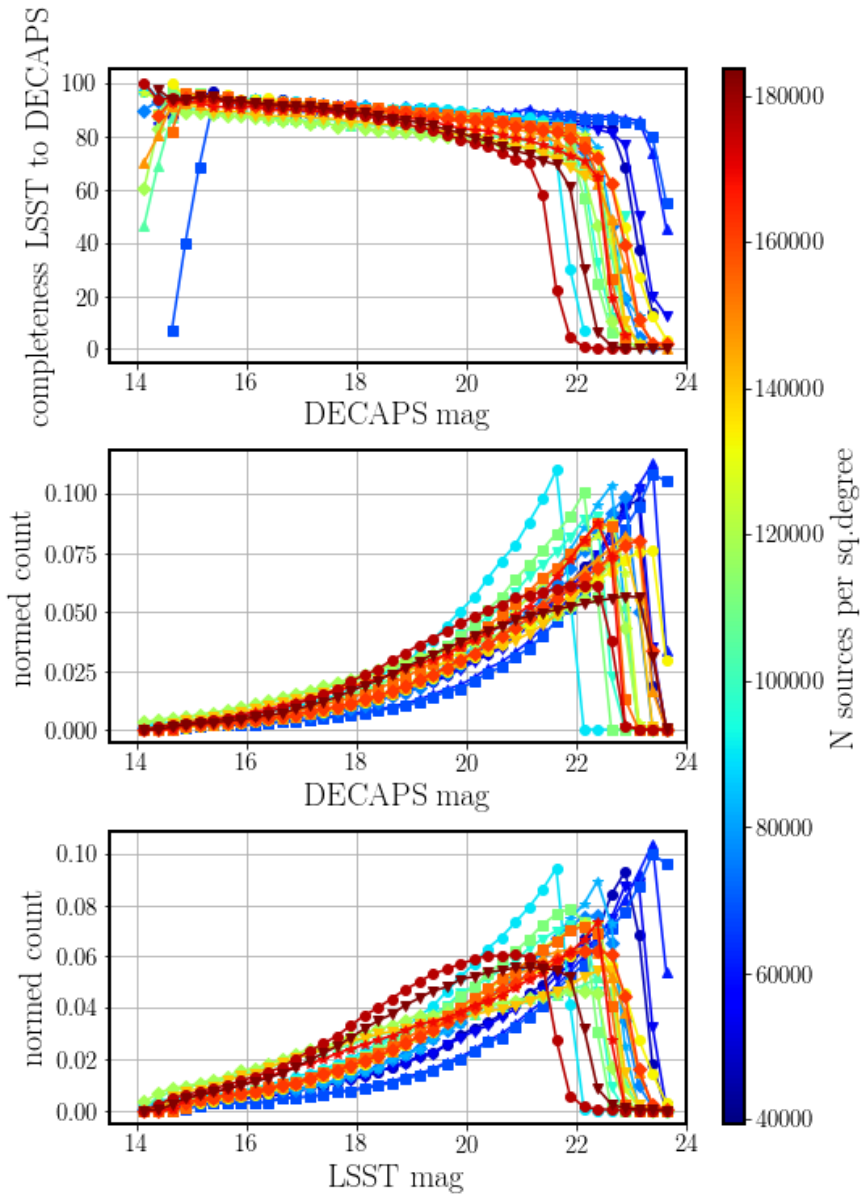


FIGURE 14: Different colors correspond to different level of stellar crowdedness, expressed in terms of number of sources per square degree (from cleaned LSST source catalogs for each visit). The top panel depicts the completeness of DECAPS sources to LSST binned along DECAPS magnitudes. The middle panel the count of cleaned DECAPS catalog, and the bottom panel the count of cleaned LSST catalog, before they are cross-matched. The completeness falls down the higher the source density.

isons.

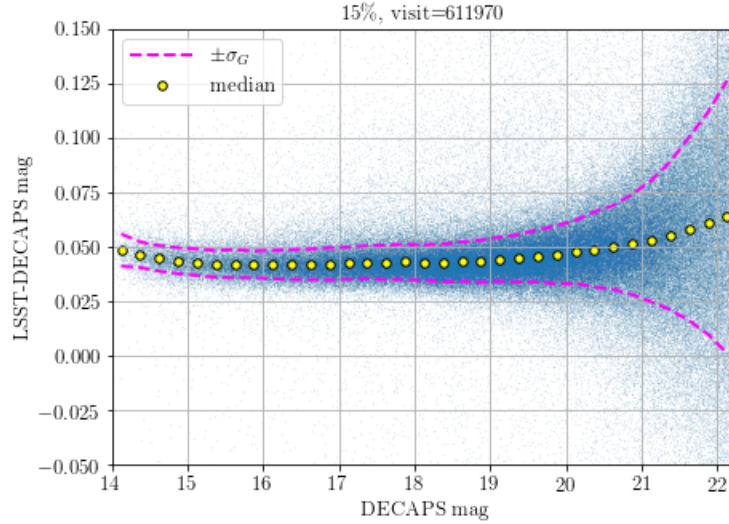


FIGURE 15: Difference in magnitudes between the DECAPS and LSST magnitudes for sources matched within 0.5 arcsec for a region in top 15% density (611970). While in calculating completeness apart from spatial proximity we require sources to be within 0.5 mag to constitute a ‘match’, here we did not exclude any outliers in calculating the median and σ_G , since these statistics are insensitive to outliers. We overplot the median with yellow circles, and the $\pm\sigma_G$ envelope - the measure of scatter based on the interquartile range. The offset between LSST and DECAPS is on the level of 0.05 mag. The same quantities plotted for all fields can be shown on Fig. 17

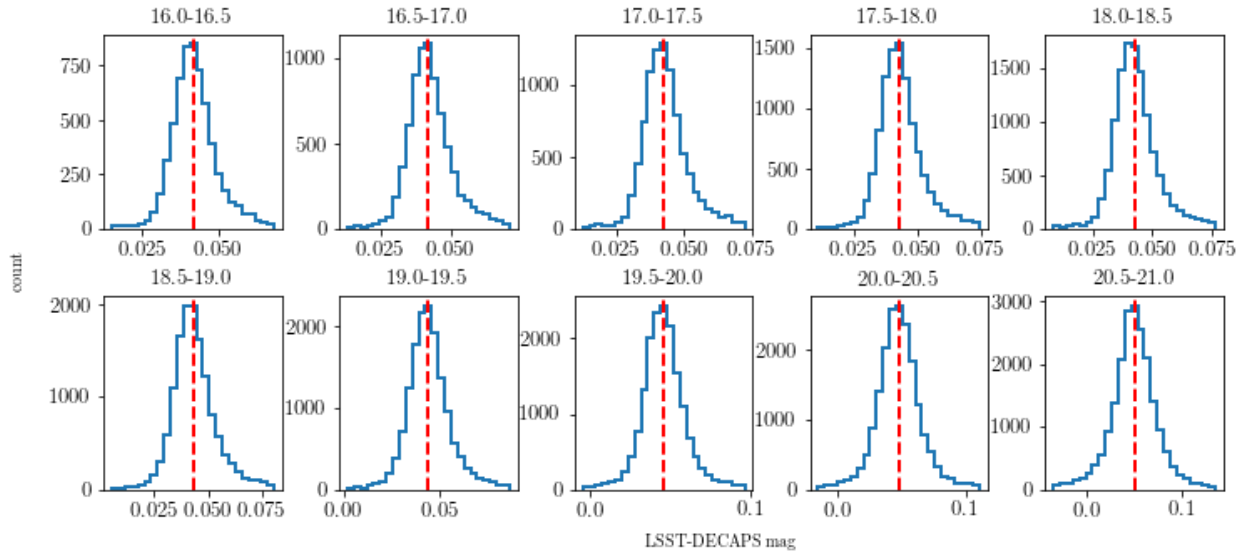


FIGURE 16: Cross-section of Fig. 17, showing the histogram of magnitude difference per DECAPS magnitude bin, plotting the median as vertical line, with each histogram limited between $\pm 4\sigma_G$.

For two fields per stellar density regime (5%, 10%, 15%, 20%) we found visits at exactly the

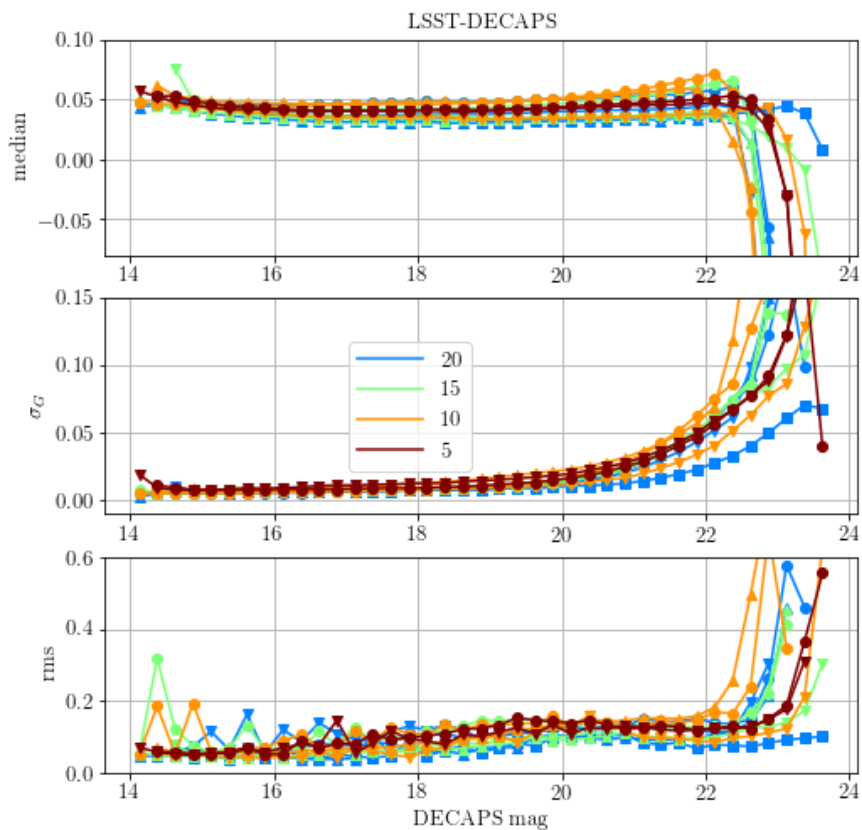


FIGURE 17: Median, σ_G , and root-mean-square calculated for fields of different stellar density. Fields at different locations but similar source densities have the same color, but different markers.

TABLE 8: Listing of pairs of visits at two different epochs, two per density regime. RA and DEC are in degrees. The separation in arcseconds is between the center of each exposure field of view. The last column shows the time difference between the two visits.

visit1	ra1	dec1	magzero1	visit2	ra2	dec2	magzero2	d2d [arcsec]
525904	140.5531	-51.24729	29.47	527300	140.5534	-51.24555	29.459	6.3
525920	143.2337	-51.44724	29.4465	527296	143.2329	-51.446	29.259	4.8
525846	133.5462	-44.27313	29.738	530012	133.5508	-44.27435	29.783	12.6
525879	137.6415	-54.08343	29.775	530032	137.642	-54.08628	29.734	10.3
525837	131.5622	-48.59523	30.011	527246	131.5601	-48.59695	29.699	7.9
525838	132.5935	-50.30486	29.344	527247	132.5894	-50.30705	28.991	12.3
525814	126.4261	-43.06979	29.4545	529974	126.4192	-43.07151	29.466	19.2
525900	140.6165	-48.15003	29.772	529989	140.6162	-48.15212	29.809	7.6

same location, filter and exposure time, but different epoch (see Table 8). This allowed to compare the spread in photometry epoch-to-epoch within DECAPS, and LSST. We illustrate that plotting the magnitude differences on Figs. 18 and 19, and the summary of the spread of photometric difference as a function of magnitude on Figs. 20 and 21.

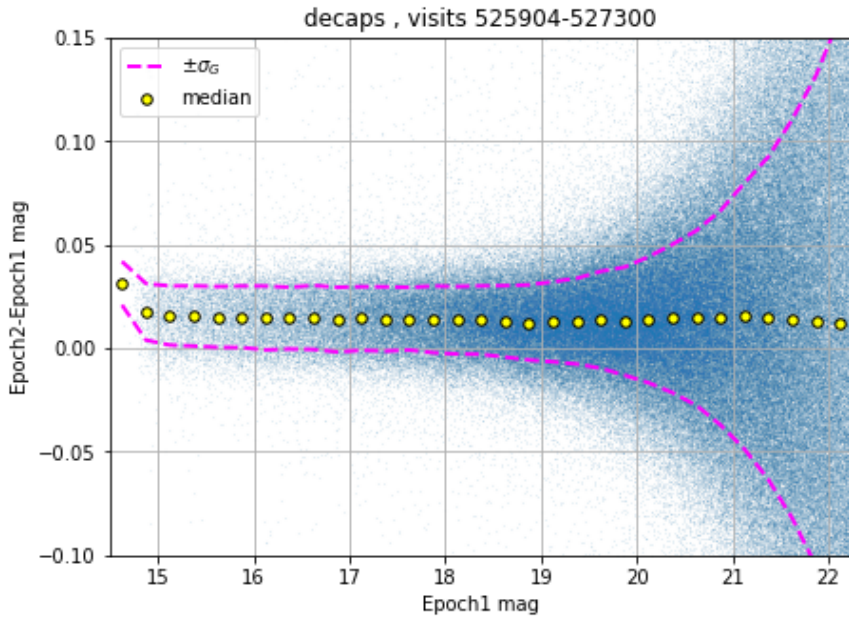


FIGURE 18: Similarly to Fig. 15, scatter plot of the magnitude difference between the two epochal visits (525904, 527300) to the same sky region, separated by 2.95 days, processed by DECAPS. The magnitude difference is shown for all sources cross-matched between the two epochs, with a match within 0.5 arcseconds - there is no selection on magnitude difference, but 0.5 mag (used for completeness) is well beyond the bounds of the plot, and would only cut the outliers to which neither median nor σ_G (interquartile-based estimate of the spread) are not sensitive. We overplot the $\pm\sigma_G$ envelope, and the median of each of 0.25 mag bins, spread between 14.5 and 22.5 mag.

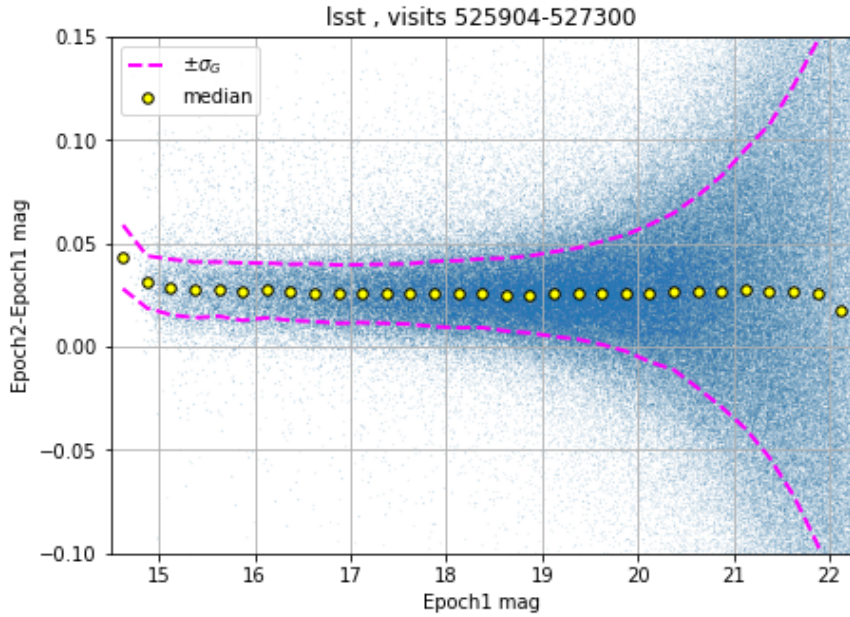


FIGURE 19: The same as Fig. 18, but for LSST processing of two visits to the same region, at two different epochs.

The statistical spread epoch-to-epoch is on the level of 0.1 mag, which is almost twice as large as the spread between processing of the same field by two different pipelines (0.05 mag).

6 Future work

6.1 LSST Processing of StarFast Simulated Sky

An independent way to further test the performance of the LSST Science Pipelines is to use the simulated sky images, where the true position and brightness of each source is known. This would put the measure of source detection completeness, photometric and astrometric precision on an absolute scale. We already tested a StarFast image simulator⁹, and confirmed that it can successfully simulate a region of the sky seeded with known stellar population.

⁹<https://dmtm-012.lsst.io>

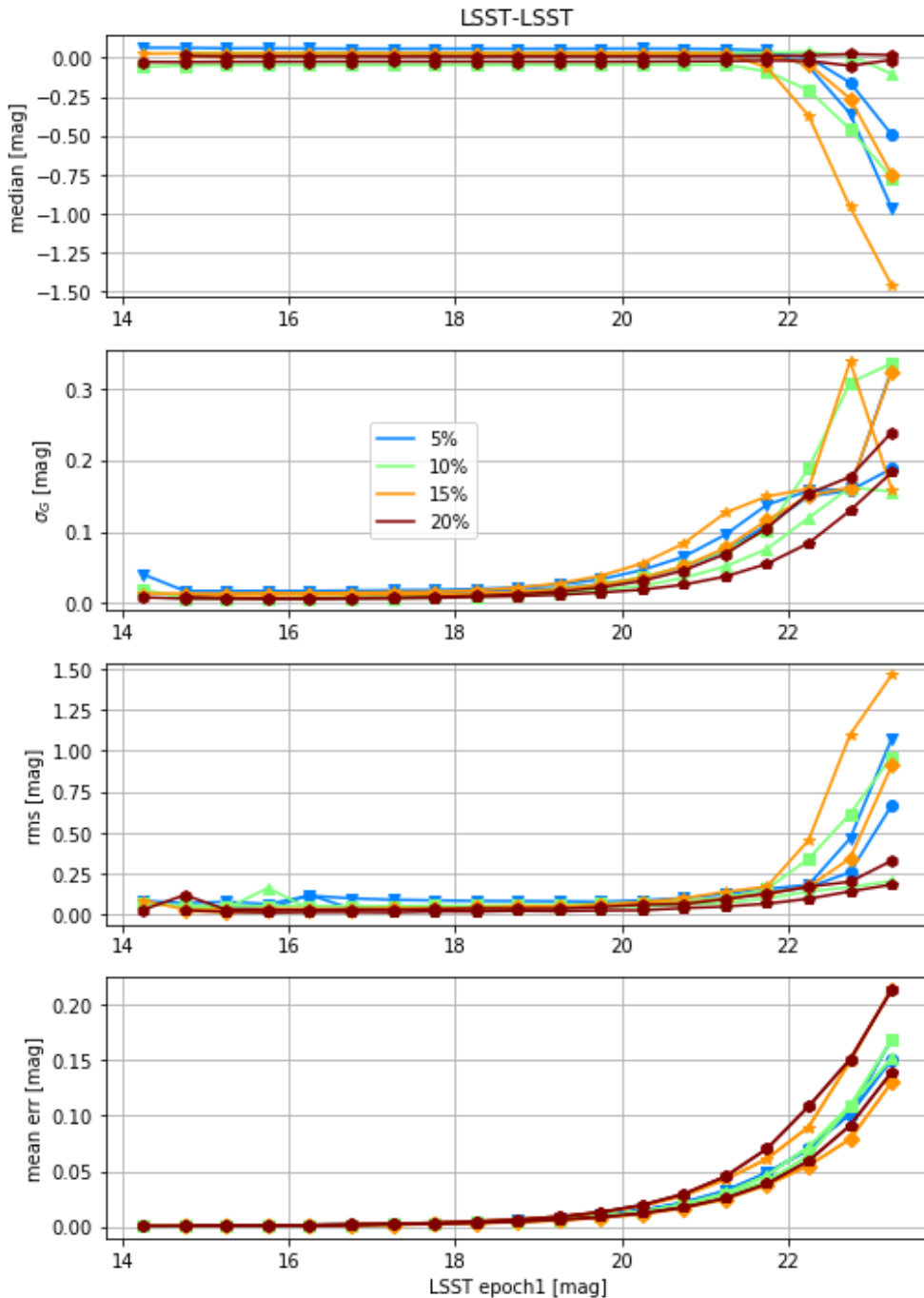


FIGURE 20: Median, σ_G , rms, and median error, for two epochs processed by LSST. Color corresponds to density level, and marker to the same visit pair across panels.

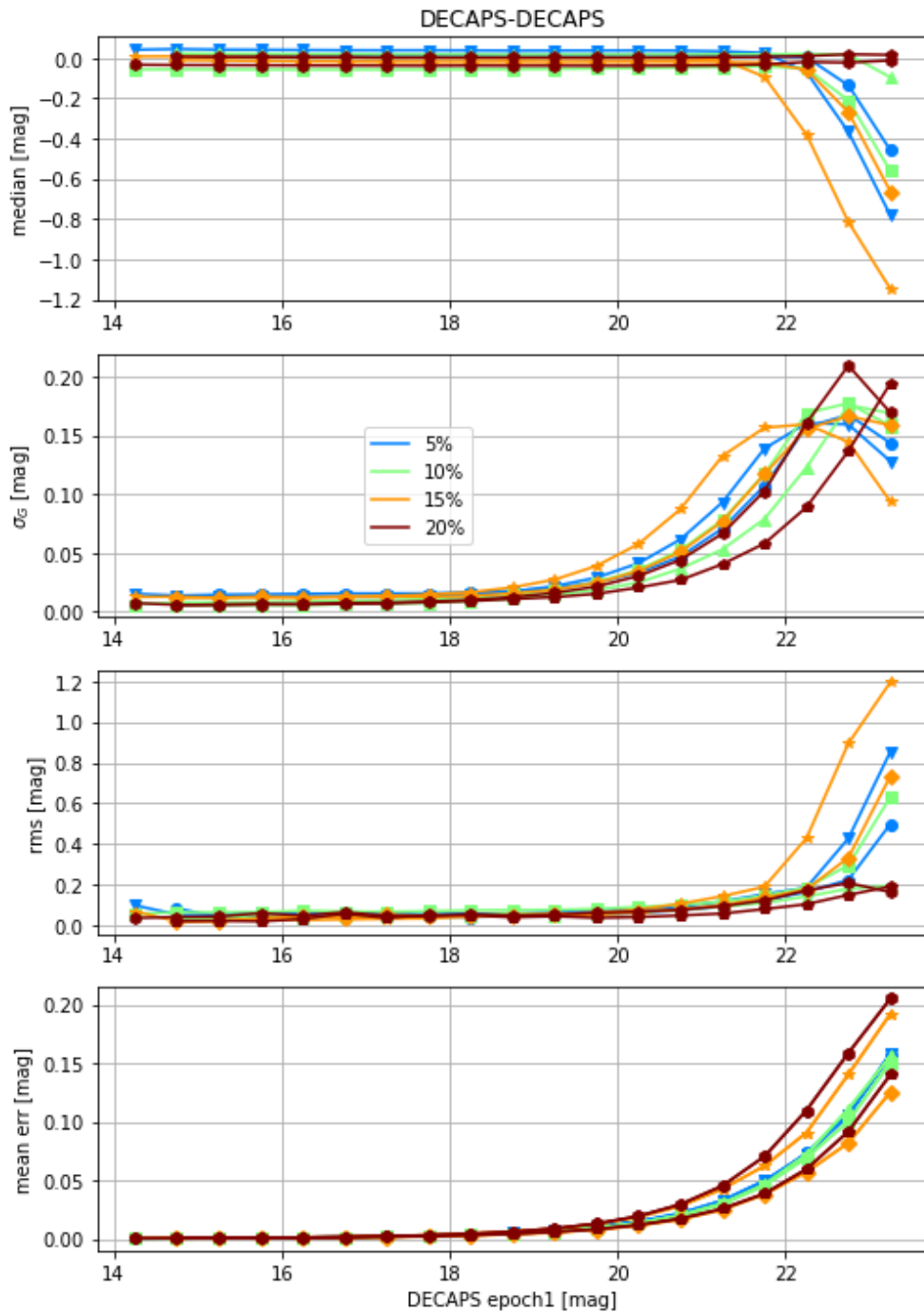


FIGURE 21: Similar to Fig. 20, but for DECAPS processing.

6.2 Other LSST-DECAPS tests: w-color

An independent test of the quality of photometry would be to consider the width of the stellar locus ('w-color') on the g-r vs r-i color-color plot. This could be used to test internal consistency of LSST and DECAPS photometry.

6.3 Astrometry

Here we consider the accuracy of position measurement. There are three possible combinations of catalogs : LSST-DECAPS data for the same epoch (22), LSST-LSST and DECAPS-DECAPS data for different epochs. We plot the difference in RA, DEC measurement of matched sources between the two source catalogs.

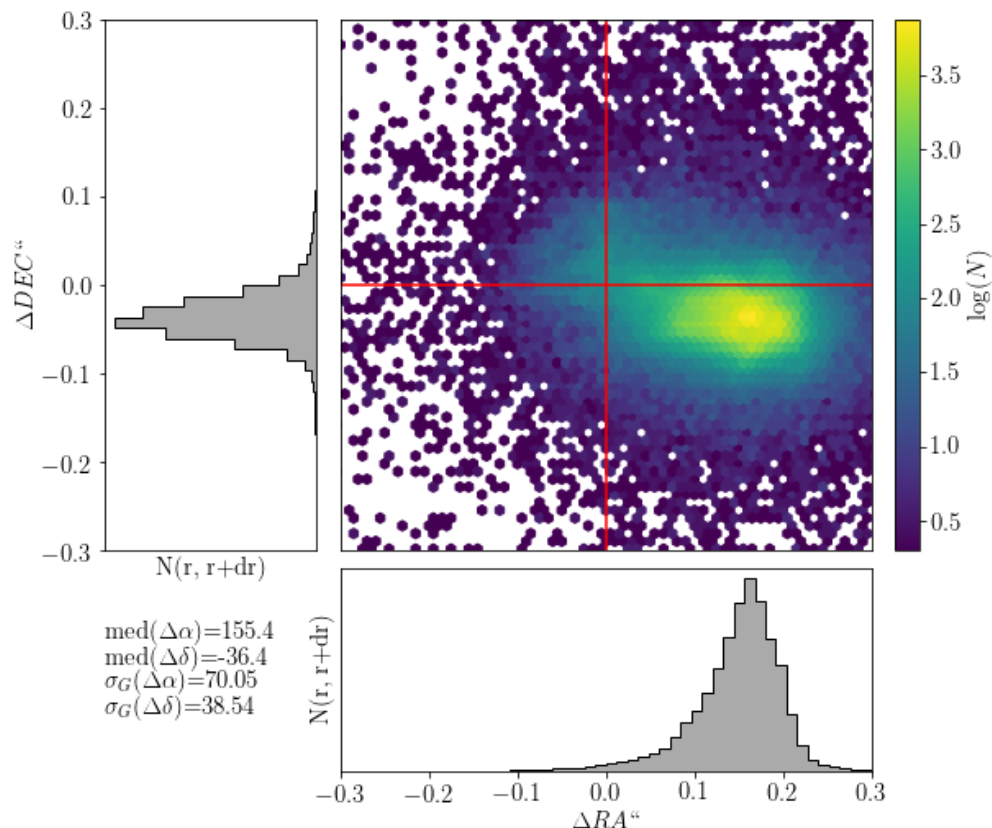


FIGURE 22: The difference in RA,DEC for visit 525904 , between LSST and DECAPS processing (402270 detected sources in the clean LSST catalog). We tested that for other visits (525920, 525846, 525879, 525837, 525838, 525814, 525900), and in all cases the offset position and magnitude remains the same - see Table 9

TABLE 9: The difference in RA,DEC for the same visit analyzed by LSST and DECAPS. Each row corresponds to a separate visit, which correspond to different stellar density. All measured quantities are in miliarcseconds.

visit	median($\Delta\alpha$)	median($\Delta\delta$)	$\sigma_G(\Delta\alpha)$	$\sigma_G(\Delta\delta)$
525904	155.49	-36.46	70.06	38.55
525920	130.45	-27.53	72.83	43.88
525846	105.62	-51.71	42.49	30.04
525879	131.93	-42.62	138.58	75.68
525837	96.01	-47.93	65.17	36.6
525838	124.9	-68.92	59.56	33.99
525814	39.99	-29.87	47.26	29.72
525900	127.61	-32.38	54.81	33.67
527300	146.26	-38.73	56.49	25.48
527296	120.47	-26.98	41.65	27.14
530012	111.21	-51.38	35.01	28.34
530032	126.69	-47.85	115.02	65.23
527246	88.38	-49.06	45.87	30.6
527247	110.44	-66.18	43.15	29.71
529974	49.13	-30.91	48.55	28.95
529989	126.51	-33.77	52.12	28.33

TABLE 10: The difference in RA,DEC for various visits, between LSST processing of fields at the same location, but observed at different times (see Table 8 for summary). All measured quantities are in miliarcseconds.

visit1	visit2	median($\Delta\alpha$)	median($\Delta\delta$)	$\sigma_G(\Delta\alpha)$	$\sigma_G(\Delta\delta)$
525904	527300	3.35	-1.21	42.94	29.81
525920	527296	5.52	-2.73	59.46	38.06
525846	530012	-1.15	-0.15	58.45	41.82
525879	530032	0.63	-0.48	40.31	26.76
525837	527246	2.9	-1.32	58.91	40.45
525838	527247	4.01	-2.45	95.15	61.5
525814	529974	-3.03	0.7	55.24	39.31
525900	529989	2.61	0.45	69.36	47.08

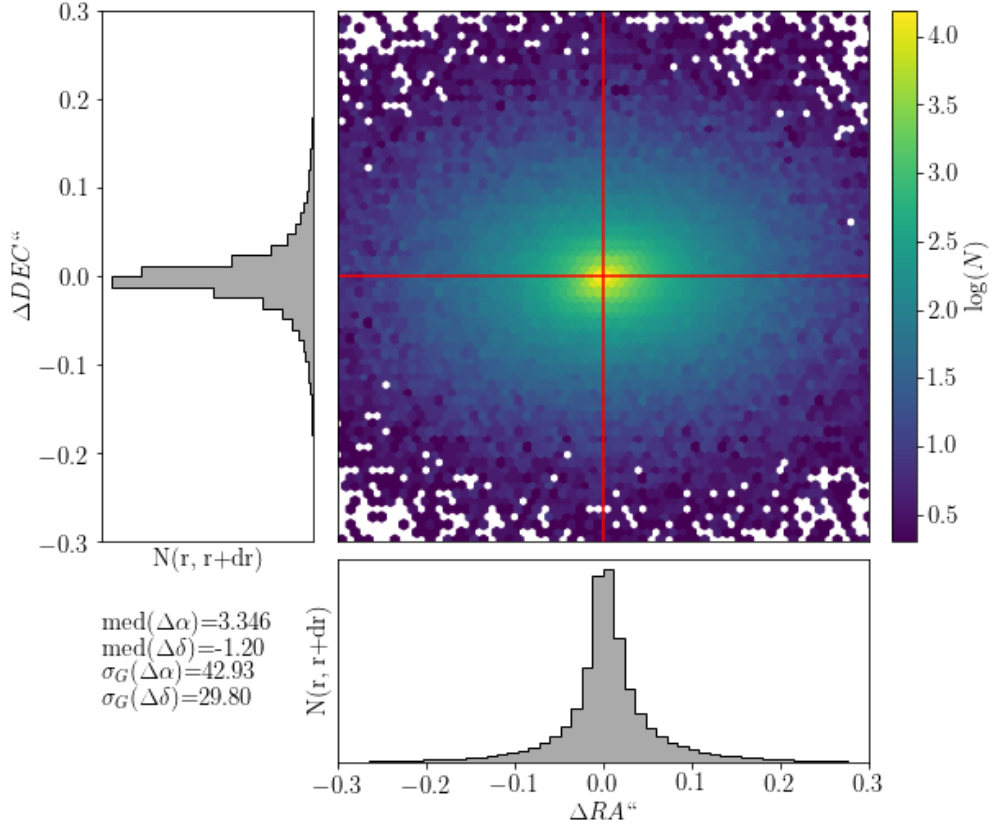


FIGURE 23: The difference in RA,DEC for visits 525904,527300: a pair of visits at the same location, but different epochs, both processed by the LSST Science Pipelines. One has 402270, and the other 366871 detected sources in the clean LSST catalog. We tested that for other visit pairs the $\Delta\alpha$, $\Delta\delta$ are all centered on zero with similar spread, the results summarized in the Table 10

TABLE 11: The difference in RA,DEC for various visits, between DECAPS processing of fields at the same location, but observed at different times (see Table 8 for summary). All measured quantities are in miliarcseconds. See Table 10 for the equivalent visits processed by LSST.

visit1	visit2	median($\Delta\alpha$)	median($\Delta\delta$)	$\sigma_G(\Delta\alpha)$	$\sigma_G(\Delta\delta)$
525904	527300	-4.46	-3.21	77.09	52.28
525920	527296	-1.46	-1.84	119.16	75.3
525846	530012	3.42	-1.07	72.7	53.69
525879	530032	-2.2	-5.44	97.02	61.59
525837	527246	-4.23	-3.1	127.93	87.24
525838	527247	-9.05	-1.28	177.23	116.0
525814	529974	4.65	-0.92	73.56	50.66
525900	529989	-0.04	-3.21	80.07	54.0

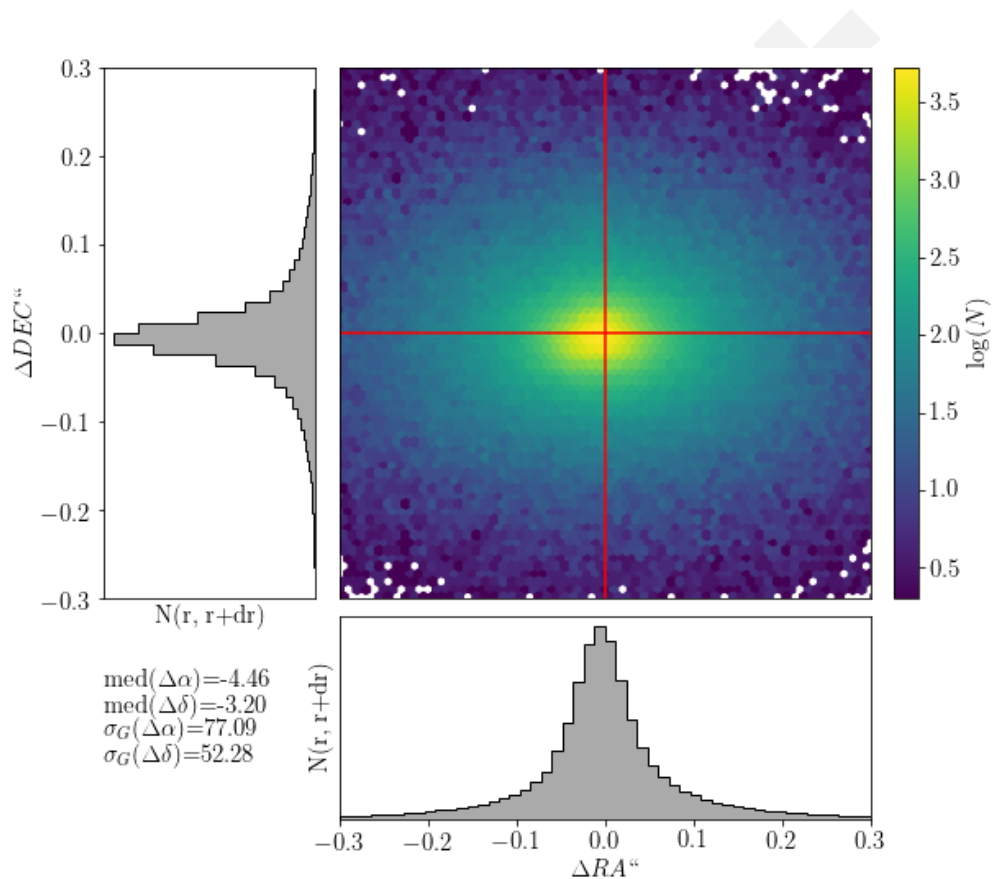


FIGURE 24: The difference in RA,DEC for visits 525904,527300 - same location, different epochs, from DECAPS source catalogs. The spread of $\Delta\alpha$, $\Delta\delta$ is wider than for equivalent visit pairs processed by the LSST Science Pipelines - see Table 11

	archive	$ $	b	TRILEGAL	MAF	DAO
c4d_140624_080728_ooi_r		13.70	-4.43	7,960,511	2,650,680	498,760
c4d_170428_094150_ooi_g		356.86	-3.90	39,852,793	4,587,804	375,980
c4d_170501_055757_ooi_g		356.26	5.05	16,352,821	2,659,968	285,630
c4d_170504_084722_ooi_g		4.26	5.15	15,586,874	2,833,740	561,795

TABLE 12: Source density comparison for 1% density level : TRILEGAL, DAO and MAF columns contain stellar counts from TRILEGAL simulation , DAOStarFinder based on DECam data, and MAF simulation, respectively. All counts are in stars per square degree.

A Appendix A: TRILEGAL and DAOPhot

A.1 DAOStarFinder source detection

Per each density regime, we performed source extraction with DAOStarFinder¹⁰. This tool uses a classic DAOFIND algorithm [11], and we used it to verify the plausibility of the MAF source densities using real data. We performed a straightforward DAOPhot source extraction setting the detection threshold at 5σ level, setting the detection threshold at 5σ .

A.2 TRILEGAL queries

For the same regions of the sky we also obtained TRILEGAL¹¹ simulation results, keeping $r < 24.5$ sources, with all other run settings as default.

A.3 Comparison of MAF, DAOStarFinder, and TRILEGAL counts

We used the number of sources per TRILEGAL output file, and scaled it to the degree level to compare with MAF and DAO. The results are shown in Tables 12, 13 , 14 , 15 for 1%,5%,20% and 50 % density levels.

References

[1] Bosch, J., et al. 2017, ArXiv e-prints

[2] Hogg, D. W. 2001, The Astronomical Journal, 121, 1207

¹⁰<http://photutils.readthedocs.io/en/stable/photutils/detection.html>

¹¹<http://stev.oapd.inaf.it/cgi-bin/trilegal>

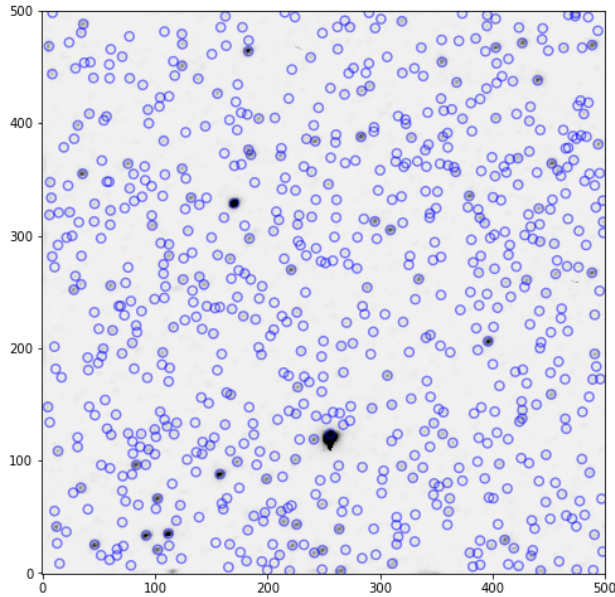


FIGURE 25: 500x500 pixels (135x135 arcseconds) subregion of DECam field c4d_170504_084722_ooi_g, a top 1% density region. With DAOPhot threshold set at 5σ , we detected 722 sources in this postage stamp miniature, corresponding to the area of 0.001406 sq degrees, which translates to 513,422 sources per square degree. At the same coordinates, MAF density is 2,833,740 sources per square degree, and TRILEGAL density is 15,586,874 sources per square degree.

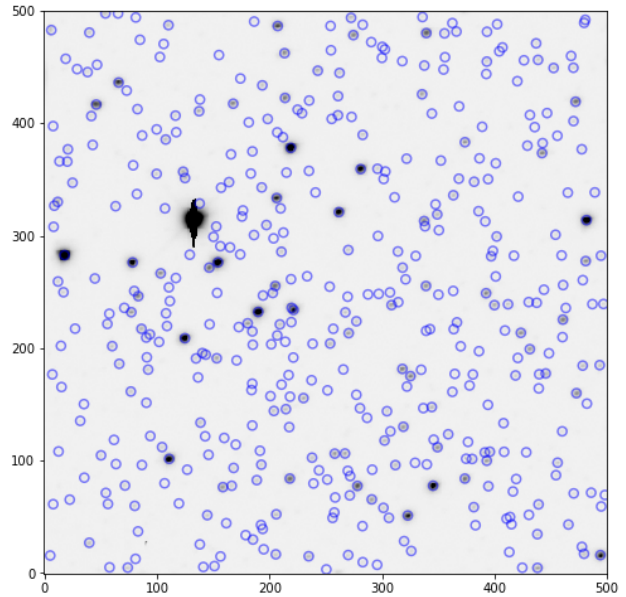


FIGURE 26: 500x500 pixels (135x135 arcseconds) subregion of DECam field c4d_170429_035748_ooi_g, with 436 detected sources, in the 5 % density region. The same DAOPhot settings as Fig. 25. That many sources in an area of 0.001406 sq degrees, translates to 310,044 sources per square degree. At the same coordinates, MAF density is 807,156 sources per square degree, and TRILEGAL density is 1,870,414 sources per square degree.

archive	I	b	TRILEGAL	MAF	DAO
c4d_160316_065235_ooi_g	301.42	3.40	1,606,135	591,336	179,277
c4d_160825_231905_ooi_g	314.05	3.08	2,564,964	589,572	127,088
c4d_170429_035748_ooi_g	310.43	-4.02	1,870,414	807,156	327,483
tu1677011	4.48	8.70	2,530,163	810,144	509,093

TABLE 13: Source density comparison for 5% density level, all columns and units as in Table 12

archive	I	b	TRILEGAL	MAF	DAO
c4d_170122_055542_ooi_g	242.43	3.77	341,343	116,856	66,282
tu1661798	351.66	20.42	183,778	118,188	44,216
tu1668579	217.04	1.21	379,319	111,096	54,004
tu2187073	312.84	14.64	184,583	107,784	60,678

TABLE 14: Source density comparison for 20% density level, all columns and units as in Table 12

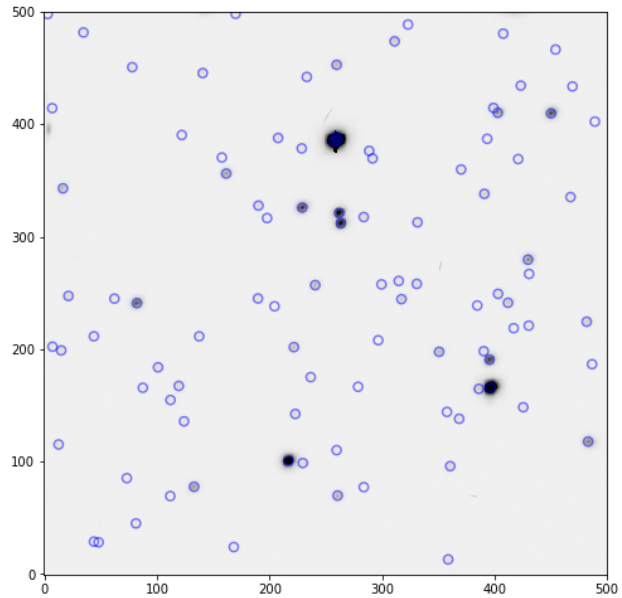


FIGURE 27: 500x500 pixels (135x135 arcseconds) subregion of DECam field c4d_170122_055542_ooi_g, with 98 detected sources, in the 20 % density region. The same DAOPhot settings as Fig. 25. That many sources in an area of 0.001406 sq degrees, translates to 69,688 sources per square degree. At the same coordinates, MAF density is 116,856 sources per square degree, and TRILEGAL density is 341,343 sources per square degree.

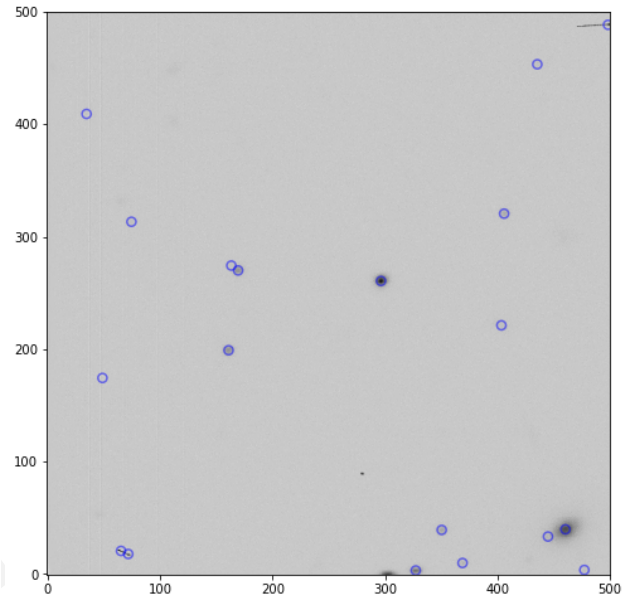


FIGURE 28: 500x500 pixels (135x135 arcseconds) subregion of DECam field c4d_160607_025052_ooi_g, with 19 detected sources, in the 50 % density region. The same DAOPhot settings as Fig. 25. That many sources in an area of 0.001406 sq degrees, translates to 13,511 sources per square degree. At the same coordinates, MAF density is 20,052 per square degree, and TRILEGAL density is 29,607 sources per square degree.

archive	I	b	TRILEGAL	MAF	DAO
c4d_150615_005257_ooi_g	344.39	41.67	27,633	21,024	12,904
c4d_160607_025052_ooi_g	2.92	41.68	29,607	20,052	13,371
c4d_160825_034122_ooi_g	345.83	1.28	18,364,268	20,268	91,177
tu2046406.fits.fz	220.89	-16.08	41,832	19,944	35,974

TABLE 15: Source density comparison for 50% density level, all columns and units as in Table 12

- [3] Lupton, R. 2005, in prep.
- [4] Lupton, R., Gunn, J. E., Ivezić, Z., Knapp, G. R., & Kent, S. 2001, in Astronomical Society of the Pacific Conference Series, Vol. 238, Astronomical Data Analysis Software and Systems X, ed. F. R. Harnden, Jr., F. A. Primini, & H. E. Payne, 269
- [5] Lupton, R. H., Ivezić, Z., & Gunn, J. 2005, in prep.
- [6] Lupton, R. H., Ivezić, Z., Gunn, J. E., Knapp, G., Strauss, M. A., & Yasuda, N. 2002, in SPIE Proceedings, Vol. 4836, Survey and Other Telescope Technologies and Discoveries, ed. J. A. Tyson & S. Wolff, 350
- [7] Narayan, G., et al. 2018, ArXiv e-prints
- [8] Olsen, K. A. G., Blum, R. D., & Rigaut, F. 2003, AJ, 126, 452
- [9] Schlaflfy, E. F., et al. 2017, ArXiv e-prints
- [10] Shaw, R. A. 2015, NOAO Data Handbook
- [11] Stetson, P. B. 1987, PASP, 99, 191